Impact of Mixing-Driven Calcite Precipitation on Solute Transport Dynamics: Insights from Laboratory Visualization and Tracer Tests Analysis

Guido González-Subiabre *, Rodrigo Pérez-Illanes, Daniela Reales-Núñez, Maarten W. Saaltink, Michela Trabucchi, Daniel Fernàndez-Garcia

Posted Date: 4 February 2026

doi: 10.20944/preprints202601.2390.v1

Keywords: mixing; calcite; precipitation; heterogeneity; solute transport; breakthrough curves

Article

Impact of Mixing-Driven Calcite Precipitation on Solute Transport Dynamics: Insights from Laboratory Visualization and Tracer Tests Analysis

Guido González-Subiabre [1,2], Rodrigo Pérez-Illanes [3], Daniela Reales-Núñez [1,2], Maarten W. Saaltink [1,2], Michela Trabucchi [1,2], and Daniel Fernàndez-Garcia [1,2]

[1] Associated Unit: Hydrogeology Group (UPC-CSIC), Jordi Girona 1-3, Barcelona, 08034, Spain
[2] Department of Civil and Environmental Engineering, Universitat Politècnica de Catalunya (UPC), Jordi Girona 1-3, Barcelona, 08034, Spain
[3] Institute of Applied Geosciences, Technische Universität Darmstadt, Darmstadt 64287, Germany
* Correspondence should be addressed to r.guido,gonzalez@gmail.com

Abstract

Understanding the effects of mixing-driven precipitation on solute transport behavior is critical for reactive transport predictions, yet its complexity, arising from the interplay of flow dynamics, solute transport, and geochemical reactions, remains a significant challenge. In particular, mineral precipitation modifies the hydraulic properties of porous media. The impact of this process on the solute transport behavior remains largely unexplored and is crucial for accurate reactive transport predictions. This study presents a controlled laboratory investigation of mixing-driven calcite precipitation (MDP) in an intermediate-scale Hele-Shaw cell, simulating a coarse-sand porous medium. The experiment allowed for direct visualization of the spatiotemporal evolution of precipitation while continuously monitoring hydraulic properties. Self-organized heterogeneities in the precipitate structure were observed, with calcite layers forming symmetric patterns aligned with the main flow, contrasting with the asymmetry predicted by a semi-analytical model under idealized conditions. Tracer tests conducted before and after precipitation demonstrated significant impacts on solute transport, including the emergence of strong anomalous transport features, such as earlier solute arrival, a distinct double peak, and pronounced tailing. These findings highlight the critical role of precipitation-induced heterogeneities in shaping transport behavior, emphasizing the need to integrate these dynamics into reactive transport models for improved predictive accuracy.

Keywords: mixing; calcite; precipitation; heterogeneity; solute transport; breakthrough curves

1. Introduction

Understanding the consequences of mixing waters with different chemical signatures is of critical importance for studies assessing the health of groundwater systems [e.g., 1–4] and engineering efforts aiming to design effective subsurface pollution control strategies [e.g., 5–7]. However, quantifying the extent of mixing in real-world hydrogeological systems is often difficult because of the generally unknown complexity of the medium heterogeneities (which translates into high uncertainty in the prediction of flow velocities) [8–11] and the impossibility of visually assessing the transport of solutes through the porous medium. Depending on the species in solution and the chemical composition of the host porous medium, the mixing of waters with different signatures can lead to the occurrence of reactions that influence the microscopic structure of the solid material and of the pore network [12–14]. Eventually, this interaction creates a feedback loop where changes in the porous medium (including changes in grain size and pore/pore-throat size distributions) now influence the groundwater flow, the extent of mixing (incomplete mixing) [15,16], and the rate of chemical reactions [13,17]. One reactive process commonly discussed in the subsurface literature is the precipitation/dissolution of carbonates

 doi:10.20944/preprints202601.2390.v1

(i.e., calcite). Various studies have discussed potential applications of this chemical process in the context of groundwater remediation [e.g., 18–21], Geological Carbon Sequestration (GCS) [e.g., 7,22–24], Enhanced Oil Recovery (EOR) [e.g., 25–28], Managed Aquifer Recharge (MAR) [e.g., 6,18,29,30] and Coastal Aquifers Management (CAM) [e.g., 5,31]. Of particular interest is the occurrence of mineral precipitation. This process has been explored in applications of pollutant remediation, with engineered mineral precipitation aiming to trap harmful chemical species (e.g., heavy metals) in order to limit their uncontrolled movement, reducing the risk of polluting freshwater sources while also facilitating their removal [18,29,32,33]. Similarly, in carbon sequestration, precipitation is employed to purposefully decrease the effective permeability of some regions in the porous medium to meet the specific objectives of a given application [7,22,23].This context serves to underline the importance of understanding the mechanisms that control the occurrence of mineral precipitation in groundwater systems as a necessary step to improve the effectiveness of subsurface engineering applications based on this process. Along this line, the Mixing-Driven Precipitation (MDP) of carbonated minerals, and the interactions that the fresh precipitate may experience with the porous medium and groundwater flow are of special interest [34–38]. In this case, as the reaction progresses towards precipitation, the mixture simultaneously flows through the medium, meaning that supersaturation — and thus the tendency for precipitation — increases downstream from the initial mixing zone [11,13,14,39]. Depending on the local flow conditions, the roughness of the grain surface, and the structure of the pore network, the mineral may nucleate and attach to the solid matrix through heterogeneous deposition, gradually transforming the substrate chemistry from the original sand grains to newly formed precipitates [34–36]. In this context, a significant knowledge gap exists regarding how mineral precipitation evolves spatially and temporally under different mixing conditions, as well as the characteristic patterns and heterogeneities emerging from the process. These aspects are crucial for understanding how precipitation impacts the effective solute transport properties of the system, particularly the quantitative metrics used to describe the transport of dissolved species (e.g., breakthrough curves). However, these effects remain largely unknown and their detailed characterization is of relevance, for example, to assist the adequate interpretation of laboratory and field-scale tracer test experiments [40], and to evaluate the conceptual formulation of numerical models aiming to describe the transport of solutes under MDP conditions [41] . As a contribution, this article builds upon the results of a novel laboratory-scale experiment in which MDP is purposefully induced to evaluate the spatiotemporal evolution of calcite precipitation and to quantify the impact of MDP on solute transport through breakthrough curves (BTCs). The experimental setup allows to monitor and visualize in real-time the spatiotemporal evolution of the precipitation process, and to quantify the influence that the fresh precipitate exerts on the porous media system by means of breakthrough curves (BTCs) measured at the system outlet. In particular, this study focuses on the precipitation of calcite ($CaCO_3$) as a test mineral, occurring in a synthetic two-dimensional homogeneous aquifer emulating a coarse sand granular system. The reactants mix due to transverse dispersion in a horizontal flow-through system with advection-dominated transport conditions. Although similar experiments exist in the literature [34–36,38], the influence that transient mineral precipitation exerts on the hydraulic and solute transport properties of the porous medium remains largely unexplored. Furthermore, experimental conditions reported in the literature have led to the precipitation of thin calcite layers [34–36], mainly due to the use of fine-grained porous media and large-scale setups that promote diffusion-dominated transport (low Péclet numbers). In contrast, variations in grain size and flow configuration can shift the balance between advection and reaction, leading to distinct precipitation patterns and heterogeneous structures. Similarly, studies analyzing breakthrough curves aiming to evaluate changes in the porous medium due to the precipitated mineral are limited, and in this work we emphasize this quantitative metric because of its high relevance for both field and experimental applications. In this sense, this work aims (i) to demonstrate that the evolution of the precipitation plume can be largely influenced by self-organized pore-scale heterogeneities driven by precipitation during the mixing process, challenging the predictions and assumptions of simplified semi-analytical reactive transport models, and (ii) to evaluate by means of

 doi:10.20944/preprints202601.2390.v1

tracer test experiments, the influence that the fresh mineral exerts on the integral transport behavior of the porous medium.

The structure of this article is as follows. The *Materials and Methods* section describes the experimental setup used for the Mixing-Driven Precipitation (MDP) and tracer test experiment, detailing the image processing technique employed to visualize the spatiotemporal evolution of calcite precipitation, along with the semi-analytical formulation used for the comparative analysis. The *Results and Discussion* section presents the main findings, including an explanation of the self-organized heterogeneous porous medium formed after MDP and an examination of the anomalous transport behavior observed in the breakthrough curve (BTC) measured after the precipitation of calcite. Finally, the article concludes with a summary of key insights from the study, emphasizing the significance of MDP and its impact on solute transport for subsurface engineering applications.

2. Materials and Methods

2.1. Experimental Setup

Experiments involving calcite precipitation and conservative tracer tests were conducted in a horizontal quasi two-dimensional tank fabricated with plexiglass, with inner dimensions of 26.5 cm in length (L), 20 cm in width (W), and 1 cm in height (H) (Figure 1a). The tank was wet-packed with spherical glass beads (d=2mm of diameter) and initially filled with deionized water (Milli-Q). The tank featured eight inlet and outlet ports, evenly spaced 2 cm apart, aiming to provide uniform flow conditions. In the inlet, four ports were connected to a 4-channel flow cell and a mini-pulse peristaltic pump (Gilson Minipulse 3 Peristaltic Pump). The other four inlet ports were connected to a separate 4-channel flow cell and pump of the same characteristics. The outlet ports of the tank were bifurcated and organized into two separate major outlets, each grouped by a 4-channel cell, followed by a pH/temperature electrode (pH/ATC Electrode BNC 8-PIN) and a Calcium Ion Selective Electrode (Thermo Fisher Scientific) connected in series after the cell. Fluorescein tracer tests were performed in order to characterize the conservative transport properties of the system. Concentrations were measured with an Albillia FL24 fluorometer that linked both outlet flow cells into a single outflow connection (purple line in Figure 1a), providing an integral breakthrough curve for the system. During the calcite precipitation experiment, potential changes in the hydraulic conductivity of the aquifer were monitored by means of two sets of Keller Series PD 23 pressure transducers installed at the inlet and outlet of the tank, which were also complemented with piezometers for comparison. The evolution of the freshly precipitated calcite was monitored via image analysis. The experimental setup was placed inside a darkroom aiming to prevent external light interference (Figure 1b), equipped with two distinct light sources for visualization. For the experiment of calcite precipitation, a 1550 Lm, 20W Downlight LED was positioned above the tank and reflected light intensity was used to monitor the evolution of the precipitate. For the fluorescein tracer tests, violet UV light combined with a green MidOpt BP525-67 filter was employed. Images were taken with a Nikon D7100 camera, paired with a Tamron SP AF17-50mm F/2.8 XR Di II LD Aspherical (IF) Model A16 lens. Throughout the experiment, a continuous monitoring was conducted for the pressure transducers, calcium probe and fluorometer measured every 1 second, pH every 5 seconds, photographs were taken every 30 seconds, and piezometers every 10 minutes. The real view of the experimental setup in the laboratory is shown in Supplementary Material (Figure S1).

 doi:10.20944/preprints202601.2390.v1

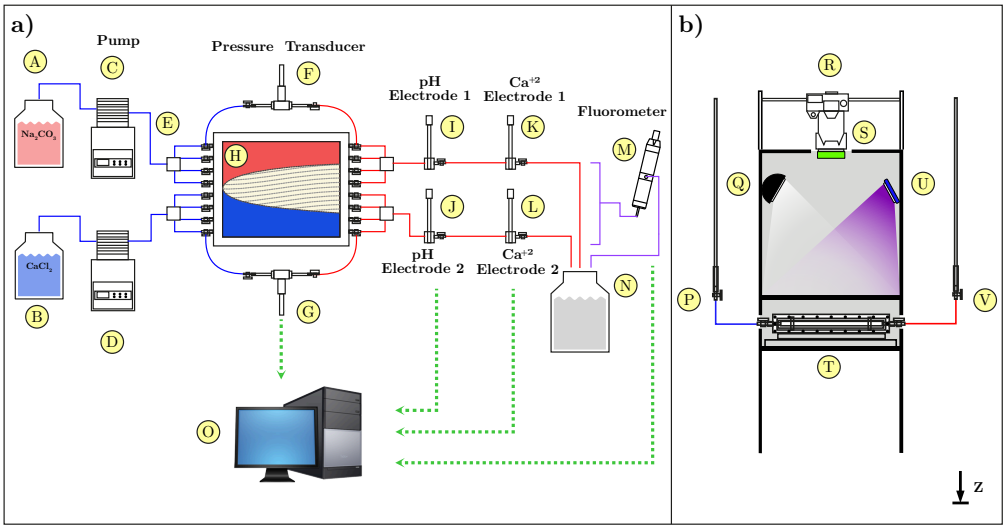

Figure 1. Top and side views of the experimental setup. Inlet flow lines: blue; outlet flow lines: red; fluorometer flow lines: violet; computer connection: green. Panel a): top view of the experimental setup where A) and B) are the containers with the inflow solutions, C) and D) peristaltic pumps. E) 4-channel cells, F) and G) pressure transducers, H) horizontal two-dimensional tank, I) and J) pH electrodes, K) and L) calcium electrodes, M) fluorometer, N) container for collecting outflow solutions, O) data logging computer. Panel b): side view of the experimental setup where P) left piezometer, Q) UV light, R) Nikon D7100 camera, S) green MidOpt BP525-67 filter, T) horizontal two-dimensional tank, U) LED light, V) right piezometer.

2.2. Initial and Boundary Conditions

Precipitation and tracer test experiments were conducted under advection-dominated transport conditions, supported by a grain Péclet number of $\mathrm{Pe} = vd/D = 523$, with v the flow velocity ($v = 2.62 \times 10^{-4}$ m/s) calculated from the total inflow rate ($Q = 1.78 \times 10^{-7}$ m^3/s), the cross-sectional area ($A = 2 \times 10^{-3}$m^2), and the initial porosity $\phi_0 = 0.34$ (experimentally determined value), d is the diameter of the glass beads in the experiment ($d = 2$mm), and D the molecular diffusion coefficient of water ($D = 1 \times 10^{-9}$m^2/s) [42]. The initial hydraulic conductivity (K_0) of the system was estimated to be $K_0 = 145.4$m/d, obtained from applying Darcy's law with the hydraulic parameters shown in Table S1 in Supplementary Material. The initial porosity ϕ_0 was determined by converting the weight of the glass beads used to fill the tank into an equivalent volume, based on the average density of glass (1g/cm^3, Labbox Labware, S.L). In terms of the flow boundary conditions, a prescribed flow boundary was established at the system entry with constant inflow rate Q, and for the system outlet a constant head boundary condition was imposed (0.9 m above the tank elevation) which was defined by trial an error in the laboratory, aiming to create a moderate hydraulic gradient with respect to the piezometric head provided by the prescribed inflow boundary.

2.3. Mixing-Driven Precipitation (MDP) and Tracer Test Experiments

The whole experimental activity lasted 630 minutes and was divided into 6 stages (Figure 2, Table S2 in Supplementary Material): a) injection of deionized water, b) initial conservative tracer test T_1, c) MDP (injection of inflow solutions W_1 and W_2 in Table 1), d) injection of a calcite-equilibrated solution (W_3 in Table 1), e) second conservative tracer test T_2, and f) calcite dissolution (injection of HCl 10%). During the first 20 minutes, deionized water was injected into the tank to achieve steady-state flow conditions (Figure 2a). This stage was followed by the first tracer test T_1, whose purpose was to obtain the initial transport conditions of the system through the breakthrough curve (BTC). During this test, a solution containing fluorescein (with concentration c_f= 3 mg/l) was injected over a 10-minute period (Figure 2b), followed by a 1 hour and 30-minute purge with distilled water. Subsequently, we conducted the MDP experiment for 120 minutes (Figure 2c), during which synthetic solutions

 doi:10.20944/preprints202601.2390.v1

of 0.05mol/kgw $CaCl_2$ (W_1) and 0.1mol/kgw Na_2CO_3 (W_2) (Table 1) were simultaneously injected into the tank, in parallel. The concentrations were chosen taking into account characteristic values reported in previous studies [34,35]. Following this stage, a solution equilibrated with respect to calcite (W_3) was introduced over a 60-minute period in order to reach geochemical equilibrium in the system (Figure 2d). The experiment continued with the second tracer test T_2 whose objective was to capture differences in the BTC consequence of the freshly formed calcite after the MDP stage. It was carried out using water in equilibrium with calcite (W_3) instead of deionized water to avoid further precipitation (Figure 2e). To conclude the experimental activities, a 10% HCl solution was introduced for a 210-minute period in order to dissolve the layer of calcite (Figure 2f), which allowed to obtain an estimation of the total amount of precipitation.

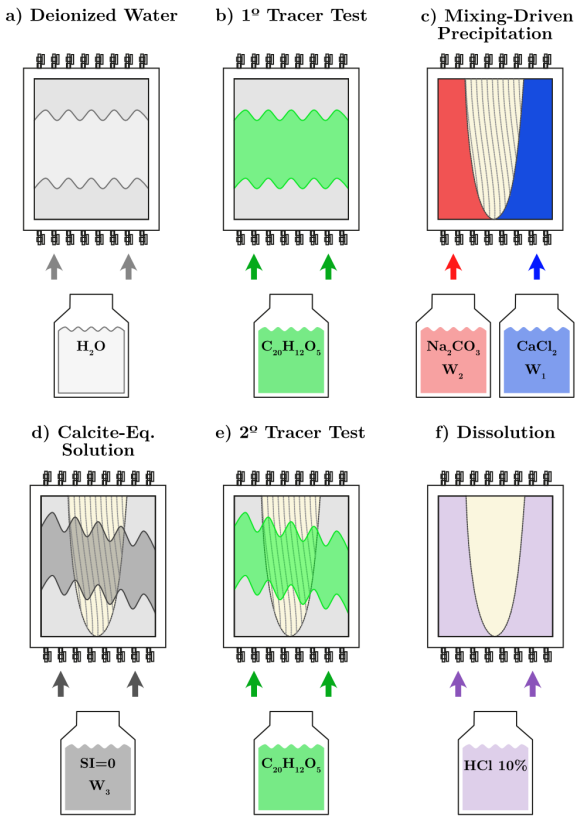

Figure 2. Detailed procedure conducted throughout the experiment: a) injection of deionized water, b) first tracer test T_1, c) Mixing-Driven Precipitation (MDP) experiment, d) injection of calcite-equilibrated solution W_3, e) second tracer test T_2, f) dissolution of the layer of calcite using a 10% HCl solution.

Table 1. Chemical properties of the solutions employed in the experiment.

Properties	Units	W_1 ($CaCl_2$)	W_2 (Na_2CO_3)	W_3 (Eq. Calcite)
pH	–	6.8	11.3	11.046
Density (*)	g/cm^3	1.00250	1.00277	1.00306
Ionic strength (*)	mol/kgw	1.5×10^{-1}	2.971×10^{-1}	1.235×10^{-1}
Temperature	^oC	21.3	21.3	21.3
SI Calcite (*)	–	-3.95	–	0
$P(CO_2)$	atm	3.16×10^{-4}	3.16×10^{-4}	3.16×10^{-4}
C (*)	mol/kgw	1.58×10^{-7}	1.007×10^{-1}	2.538×10^{-2}
Ca	mol/kgw	5×10^{-2}	–	2.016×10^{-6}
Cl	mol/kgw	1×10^{-1}	–	5×10^{-2}
Na	mol/kgw	–	2×10^{-1}	1×10^{-1}

(*) Information obtained from PHREEQC [43]. SI is saturation index. $P(CO_2)$ is the partial pressure of CO_2.

 doi:10.20944/preprints202601.2390.v1

2.4. Image Processing for Visualizing the Spatiotemporal Evolution of Calcite

The camera recorded 24-bit RGB color images during the MDP experiment, focusing on visualizing the spatiotemporal evolution of $CaCO_3$ precipitation over time. Camera settings were manually adjusted and kept constant throughout the entire experiment. A relative aperture of f/2.8, a shutter speed of 1/30 seconds, and an ISO setting of 200 were used. The images were processed using the OpenCV library in Python [44,45] following the method proposed by Schuszter et al. [46] to visualize precipitation patterns of calcite [46–48]. Images were processed following five steps: (a) converting images from raw format (NEF) to 16-bit images (TIFF); (b) cropping the images to focus on the precipitation zone which resulted in a region of interest (ROI) with resolution of 3975 x 3000 pixels, each pixel with area 6.6×10^{-3} mm^2, corresponding to a square pixel of approximately 0.081×0.081 mm in size; (c) transforming red, green and blue pixel intensity (R_I, G_I, B_I) into grayscale $\bar{I}(x,y,t)$ as

$$\bar{I} = \frac{R_\mathrm{I} + G_\mathrm{I} + B_\mathrm{I}}{3}, \tag{1}$$

which results in a single-band representation of the image with $\bar{I} \in [0, 255]$; (d) normalization of the grayscale pixel intensity $\bar{I}$ to analyze images in the range [0,1] as

$$I_n(x,y,t) = \frac{\bar{I}(x,y,t) - \bar{I}_\mathrm{back}(x,y)}{\bar{I}_\mathrm{max} - \bar{I}_\mathrm{min}}, \tag{2}$$

where $\bar{I}_\mathrm{back}(x,y)$ is the grayscale light intensity distribution of a reference image representing a blank state obtained from the steady-state flow conditions prior to the MDP experiment, and $\bar{I}_\mathrm{max}$, $\bar{I}_\mathrm{min}$ correspond respectively to the maximum and minimum grayscale intensities considering all images captured during the MDP such that their difference gives the maximum range of intensity variability; (e) and finally map the images in terms of the logarithm of the normalized intensity $I_n(x,y,t)$ for visualization and to qualitatively assess the amount of precipitation. It should be noted that $I_n(x,y,t)$ provides a qualitative representation of relative changes in $CaCO_3$ deposition. The dynamic range corresponds to the normalized optical contrast between the blank and the most intense image, as no direct calibration with calcite concentration was performed.

2.5. Semi-Analytical Model for Calcite Precipitation in Idealized Conditions

For the purposes of comparison with the MDP experiment, we developed a semi-analytical solution for the spatiotemporal distribution of calcite precipitation in a homogeneous, well-mixed, equilibrium system. The solution is based on the mixing-ratio approach discussed in De Simoni et al. [49], which determines the rate of reaction for calcite precipitation assuming idealized transport conditions, that is, instantaneous complete mixing, local equilibrium, and uniform velocity field with a negligible influence of changes in the transport properties due to the chemical process of precipitation. In this context, it has been shown that the rate of calcite precipitation can be calculated as

$$r = \phi \frac{\partial^2 C_{Ca^{2+}}}{\partial \alpha^2} \nabla^T \alpha \mathbf{D} \nabla \alpha, \tag{3}$$

where α is the mixing-ratio between the two end-members (solutions W_1 and W_2) and $C_{Ca^{2+}}$ is the concentration of the Ca^{2+} ion. The mixing-ratio α ranges between 0 and 1, and accounts for the relative contribution of one end-member to the total mixture, in this case, associated to the presence of the $CaCl_2$ solution (W_1). To exemplify, if $\alpha = 0.3$ at a given location, the concentration of the mixture at that location (without reactions) consists of 30% of the solution W_1 ($CaCl_2$) and 70% solution W_2 (Na_2CO_3). Expression (3) illustrates that the rate of reaction is composed by a chemical speciation

 doi:10.20944/preprints202601.2390.v1

coefficient ($\partial^2 C_{Ca^{2+}}/\partial\alpha^2$) and the scalar dissipation rate ($\nabla^T\alpha\mathbf{D}\nabla\alpha$). De Simoni et al. [49] showed that the mixing-ratio (α) satisfies the conservative advection-dispersion equation

$$\frac{\partial\alpha}{\partial t} = -v\frac{\partial\alpha}{\partial x} + D_L\frac{\partial^2\alpha}{\partial x^2} + D_T\frac{\partial^2\alpha}{\partial y^2}, \tag{4}$$

where D_L, D_T are the longitudinal and transverse dispersion coefficients, respectively. A transient analytical solution to equation (4), emulating idealized conditions in our experiment, was presented in the work of Wexler [50], which is also provided in Supplementary Materials (refer to Text S1, Figure S2 and Table S3). From this solution, we determined the reaction rate r by substituting $\alpha(x, y, t)$ into equation (3), where $\nabla^T\alpha\mathbf{D}\nabla\alpha$ is estimated neglecting the longitudinal gradient of the mixing-ratio $\partial\alpha/\partial x$. This assumption is valid because in the experiment the reactants necessary for calcite precipitation only meet due to mixing in the transverse direction. The chemical speciation term was obtained from a set of mixing simulations generated with the geochemical speciation code PHREEQC [43,51,52], spanning the range $\alpha \in [0, 1]$, aiming to simulate the different mixing conditions of the two end-members W_1 and W_2 (refer to Figure S3 in Supplementary Materials). From these simulations, a curve $C_{Ca^{2+}}(\alpha)$ was constructed which was later used to numerically evaluate the second derivatives $\partial^2 C_{Ca^{2+}}/\partial\alpha^2$ for a given value of α (Figure S4). As a result of mixing, PHREEQC predicted the occurrence of calcite precipitation. Some combinations of these simulations were validated experimentally to corroborate the numerical estimation of the amount of precipitated mineral (Figure S3b). With this information, it was then possible to build the spatiotemporal distribution of the precipitated mass of calcite predicted by the semi-analytical model, which was accumulated in time for each cell to properly depict the evolution of the mineral distribution.

3. Results and Discussion

3.1. Spatiotemporal Evolution of Calcite Precipitation

We begin analyzing the experimental results by discussing the evolution of calcite precipitation through a series of 6 images illustrating different instants of the MDP experiment, shown in Figure 3 . In Figure (a) it can be seen that calcite initially precipitates in a seemingly homogeneous symmetric manner ($\log(I_n) \sim [-1.4, -1.2]$), extending across the entire precipitation front. In Figure (b), small in-situ precipitation nuclei emerge at the center of the layer ($\log(I_n) \sim -0.9$). These nuclei cluster and gradually expand with time, as shown in Figure (c), forming aggregates of larger size, a dynamic that has been reported in previous studies [53–55]. As time progresses (Figures d and e), advection promotes the formation of elongated precipitation patterns, apparently following the main direction of the flow ($\log(I_n) \sim [-0.5, -0.35]$). The formation of this kind of structures has also been reported in previous studies discussing the precipitation of carbonates [56,57] and biofilm growth [55] . A more detailed view of these patterns can be seen in Figure S5. Although the linear precipitation structures observed in Figure S5 are slightly inclined relative to the horizontal flow direction, they generally follow the main orientation of the flow field. This minor deviation is attributed to small-scale variations in local flow velocity and pore connectivity within the homogeneous packing, rather than to heterogeneity in grain size or boundary effects. Similar angular patterns were observed in repeated experiments, suggesting that such orientations arise from local flow instabilities that promote preferential pathways and subsequent asymmetric precipitation fronts. For the last part of the experiment, it is observed that in between the zones of maximum calcite precipitation ($\log(I_n) > -0.35$), internal elongated structures of moderate cumulative precipitation emerge ($\log(I_n) \sim [-0.9, -0.7]$). This effect suggests the formation of preferential channels where the flow and transport will concentrate. Thus, an important highlight of our experiment is that the precipitation of calcite driven by transverse mixing transformed an initially homogeneous porous medium into a self-organized heterogeneous porous medium (after MDP). This transformation is characterized by a symmetric precipitation zone of calcite following a bell-shaped form, located at the middle of the tank, marked by the presence of elongated carbonate structures and preferential flow channels aligned with the main flow direction. These results illustrate that the growth

 doi:10.20944/preprints202601.2390.v1

of the calcite precipitate is heterogeneous, a characteristic primarily influenced by three major factors: (a) the natural presence of initial pore-scale heterogeneities inducing preferential flow channels, as evidenced by slight irregularities in the tracer front and minor variations in flow velocity observed during the pre-MDP tracer test (T_1), which suggest small differences in pore connectivity within the otherwise homogeneous packing, (b) the influence that these early precipitation structures exert on the flow and subsequent development of the precipitation reaction which impacts the degree of mixing of the reactants, and (c) some influence of the method for the injection of the input solutions (slightly non-uniform), which can create slight irregularities in the advancement of the precipitation front, for example, as seen in Figure S6 and Figure S7. We consider that these pore-scale differences have the potential to create macroscopic differences in the distribution of the mineral for different realizations of the experiment. Figures S6 and S7 illustrate the progression of two tracer tests (T_1 and T_2) conducted within the experimental tank before and after the Mixing-Driven Precipitation experiment (MDP). Figure S6 contains a sequence of images representing the initial stages of the tracer test, covering the first three time steps (4.45, 8.45, and 12.45 minutes), while Figure S7 includes images depicting the final stages, corresponding to the last three time steps (16.45, 20.45, and 24.45 minutes). Before MDP, the tracer test (T_1) exhibits a slightly irregular flow pattern, likely due to minor variations in the flow rate at the inlet ports and small heterogeneities that developed within the tank during the packing process. In contrast, after MDP, the tracer test (T_2) reveals the formation of strong preferential flow channels influenced by self-organized pore-scale heterogeneities resulting from precipitation during the mixing process.

3.2. Comparison with Semi-Analytical Model

The evolution of the calcite precipitation front observed in the MDP experiment was contrasted with the semi-analytical model developed for ideal mixing conditions, assuming instantaneous and complete mixing within each representative volume, local chemical equilibrium, and no impact of mineral precipitation on the flow and transport properties of the porous medium. The analytical solution is shown in Figure 3 with dashed lines. From Figure 3a to 3c the simulated calcite precipitation develops entirely within the side of the tank where the solution of $CaCl_2$ is injected. This condition persists until Figure 3d, where the plume opens only in a slight manner towards the upper side of the tank (the side injecting Na_2CO_3), ultimately predicting an asymmetric precipitation region, mainly oriented towards the side of the $CaCl_2$ solution (Figure 3f). As discussed previously, the experimental snapshot shown in Figure 3a depicts a precipitation region predominantly concentrated at the center of the tank, which is then further expanded towards the side where the Na_2CO_3 solution is injected (refer to Figure S8 in Supplementary Materials). This result suggests that the precipitation of calcite is influencing the hydraulic properties of the porous medium, thereby affecting groundwater flow, transport, and ultimately mixing. This was also illustrated in the works of Redden et al. [58] and Zhang et al. [35], who demonstrated that thin layers of calcite precipitation can significantly limit the interaction of water parcels, impeding mixing and altering the local flow conditions. This influence on the porous medium is not taken into account by the semi-analytical model. In general, one could also consider that the hydraulic changes induced by the precipitation of calcite could even modify the local properties of dispersion (i.e., dispersivities) in a manner that for now remains undetermined [59]. In contrast, the semi-analytical model assumes that dispersion properties remain constant in magnitude, and uniform throughout the domain, when in fact they might very well depend on the total amount of precipitation. This may be a reason explaining why conventional dispersion theories, which assume locally well-mixed conditions [9,13,16,60,61], generally fail to accurately predict mixing and the outcome of related chemical reactions.

 doi:10.20944/preprints202601.2390.v1

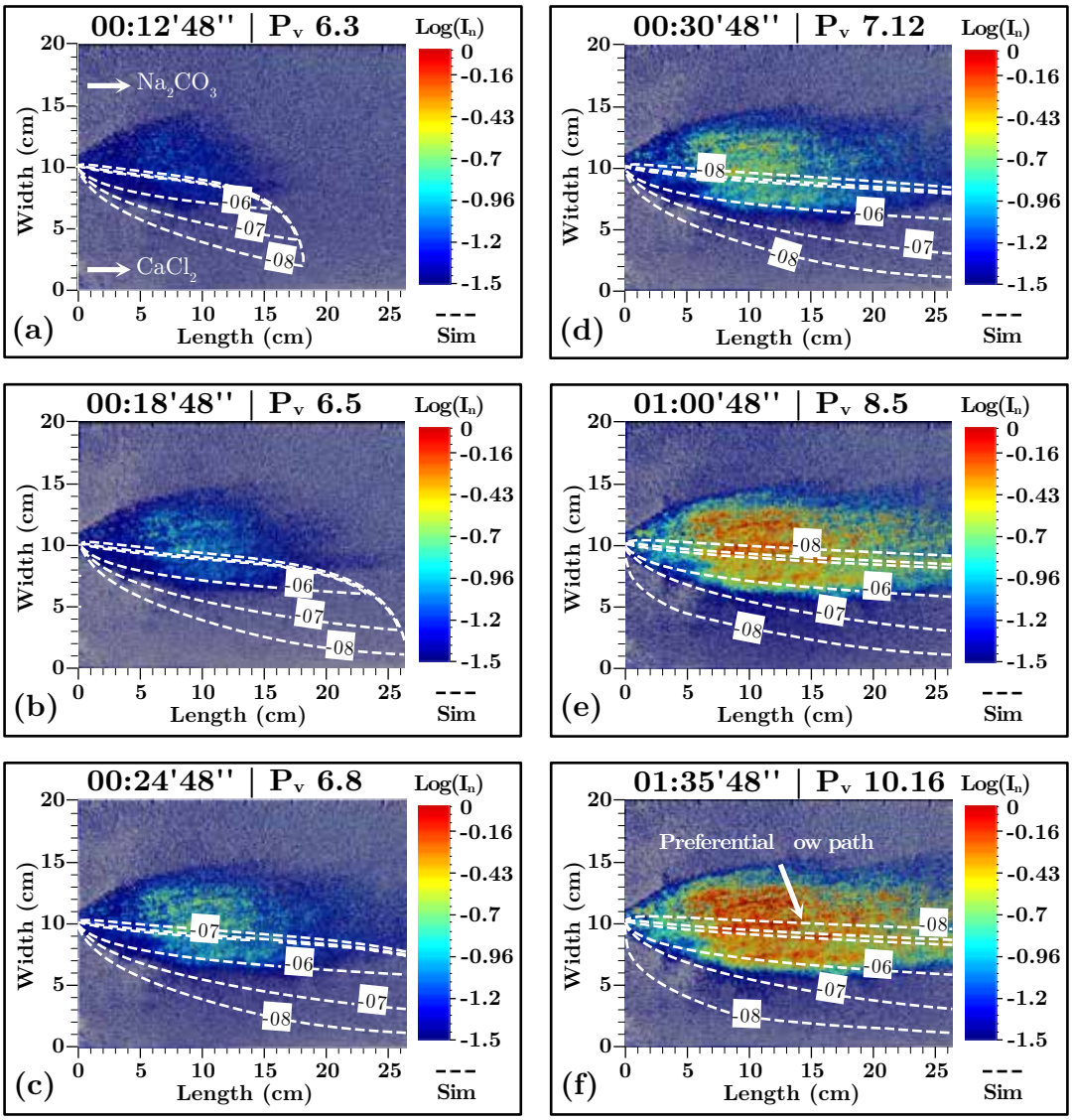

Figure 3. Evolution of calcite precipitation during the MDP experiment (colormap), and comparison with the semi-analytical model (dashed lines). The image sequence time is expressed in pore volumes, $P_v = Qt/(V\phi_0)$, where t is the time elapsed from the start of the first tracer test experiment T_1, and V is the volume of the tank. Notice that the MDP experiment started at $P_v = 5.7$ (Table S2). Images are presented in $\log(I_n)$ and the isolines of cumulative mass obtained from the semi-analytical model in log grams. The injected solutions (Na_2CO_3 and $CaCl_2$) used in the MDP experiment are indicated by white arrows in panel a).

3.3. Temporal Evolution of Calcite Precipitation Rate and Incomplete Mixing

Figure 4a presents the breakthrough curves (BTCs) of calcium measured at the system outlet during the experiment, alongside the analogous results generated by the semi-analytical model. The behavior of the BTC of electrode 2 (on the $CaCl_2$ - W_1 side) can be analyzed considering 3 stages: a) S_1, characterized by a rapid linear ascent illustrating the arrival of the calcium plume followed by a markedly moderate slope, b) S_2, characterized by a sudden increase in the slope of the calcium concentration curve, and finally c) S_3, where the slope stabilizes and becomes nearly horizontal. The initial behavior of the BTC during the S_1 stage allows us to conclude that the highest rate of calcite precipitation occurred within a short period of time at the beginning of the MDP phase. This is evidenced by the smaller slope of the BTC of calcium during this phase, which clearly increased during the S_2 stage. Furthermore, the visual inspection of Figures 3a-d also supports this idea, suggesting that the system is highly sensitive to small perturbations in the initial conditions. During S_2, the

 doi:10.20944/preprints202601.2390.v1

precipitation rate decreased with respect to S_1 illustrating a transition towards a more stable condition. Finally, in S_3, where the tank was being flushed with the solution equilibrated with calcite (W_3), the rate slope of the BTC remained stable supporting the idea that no further precipitation occurred during this phase. The semi-analytical model reveals a markedly distinct behavior. The calculated values for the concentration measured by electrode 2 (Figure 4a) rise quickly at the beginning of S_1, reaching higher values than those observed during the experimental stage S_1. The calcium output values then stabilize, achieving an earlier stable condition which is consistently maintained until S_3. This discrepancy is mainly attributed to the assumptions of made by the semi-analytical model, which tends to overestimate the total amount of precipitated calcium by assuming complete mixing and equilibrium reaction, differing from the more realistic conditions achieved in the experiment. These differences are further influenced by the changes in local porosity and the development of zones with varying hydraulic conductivities (preferential flow channels). Incomplete mixing is also evident from the analysis of the BTCs for pH obtained during the MDP experiment (Figure 4b). Before MDP, both outlet pH BTCs exhibited values of pH≈7 characteristic of the inflow of deionized water (standard values). As MDP progresses, electrode 1 experiences an increase in pH to approximately 11, characteristic of the solution of Na_2CO_3 (W_2), indicating that this solution is exiting from that side of the tank throughout the MDP phase. In contrast, electrode 2 exhibits fluctuations in pH values characterized by two peaks: the first during stage S_1 and the second at the end of S_2. The minimum pH values observed approach 7, similar to the experimentally measured value for $CaCl_2$ (W_1), which was 6.8. The maximum values of both peaks are around 8.5. These variations indicate that the peaks are the result of incomplete mixing between W_1 and W_2, suggesting the influence of local changes in the flow direction due to the precipitation of calcite.

3.4. Porosity and Permeability Reduction

The variation in porosity within the tank, resulting from calcite precipitation during the MDP experiment, was determined through a mass balance of calcium (Figure 4c). This calculation used the data from the calcium breakthrough curve (Figure 4a) considering the values obtained after the HCl injection phase. The total mass of precipitated calcite was calculated from the difference between the total outgoing calcium mass measured with the electrodes and the total injected mass of calcium, resulting in a value of 0.011 mol (around 1.1 g), which is equivalent to a volume of 0.405 cm^3. This led to only a slight reduction in the total tank porosity, from 0.34 to 0.339. Although the overall change is small, results show that an uneven spatial redistribution of this reduced volume can still induce significant local variations in permeability. Interestingly, a significant effect on permeability and transport was achieved with a relatively small amount of precipitated calcite (less than 0.1 % of the total tank volume). The variation of the effective hydraulic conductivity during MDP experiment is shown in Figure 4d. It exhibits a tendency to decrease over time, experiencing a significant variation around $P_v = 9$. Before MDP, the initial hydraulic conductivity K_0 was 145.4 m/d, decreasing to 51.78 m/d due to the precipitation of calcite.

 doi:10.20944/preprints202601.2390.v1

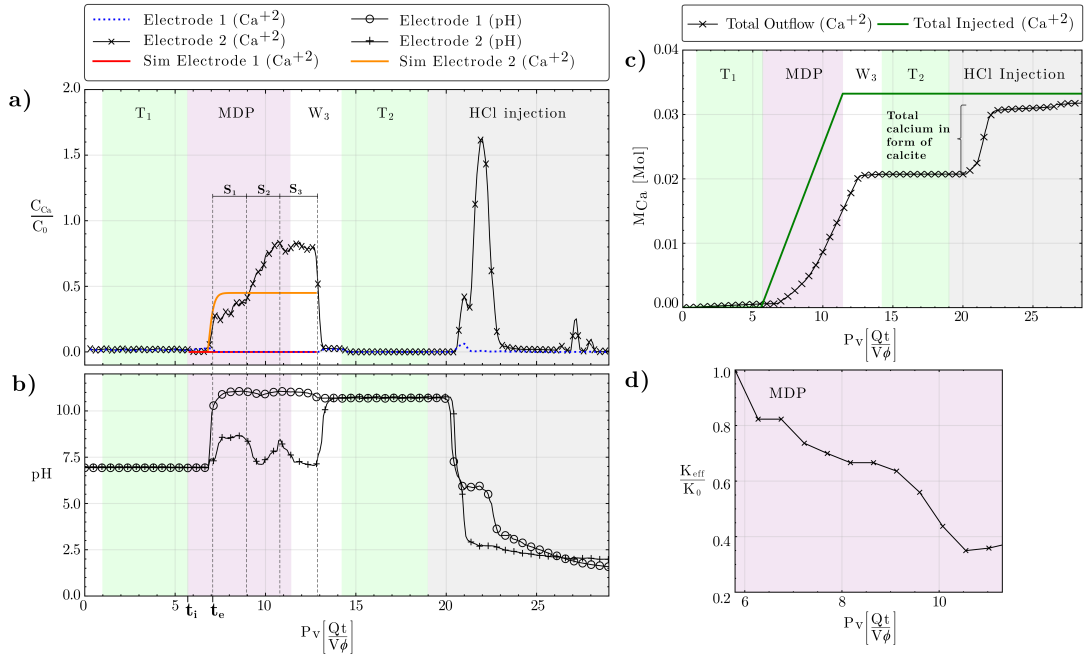

Figure 4. Quantitative experimental results. The different experimental stages are presented in zones: the first and second tracer tests are represented as T_1 and T_2, the Mixing-Driven Precipitation as MDP, and the calcite dissolution as HCl injection. a) Breakthrough curve of calcium concentration in normalized form C_{Ca}/C_0 (C_0 = 0.05 mol/kgw of W_1 in Table 1). Solid-lines represent the results of the semi-analytical model and time is expressed in pore volume P_v. S_1, S_2 and S_3 represent different identified breakthrough stages: S_1 (between P_v=7 and P_v=9), S_2 (between P_v=9 and P_v=11) and S_3 (from P_v=11 onward). b) pH measurements at both outlet ports: line with circles corresponds to Electrode 1, and line with plus-symbols represents Electrode 2. c) Mass balance of total calcium mass, where M_{Ca} represents the accumulated mass at a given instant, expressed in moles. Solid-line is obtained from the injected solution and injection flow-rate, and line with crosses is the calculated from the outflow breakthrough curves. d) Effective hydraulic conductivity relative to the initial value K_0 obtained before MDP.

3.5. Impact of MDP on Solute Transport

The effect of MDP on solute transport was analyzed through the fluorescein tracer tests obtained before and after the MDP experiment (Figure 5a,b). The first tracer test (before MDP in Figure 5a,b), displays a classical symmetric Gaussian-like distribution, indicative of Fickian behavior, which is the expected outcome for a homogeneous porous media. The BTC after the MDP experiment reveals an earlier arrival of the tracer concentration and a double-peak. The first peak concentration is considerably lower than the one obtained in the homogeneous medium, and a weaker second peak that ends in a long tail. Figure 5b highlights these differences by means of a double log scale, especially for the arrival and tailing phases of the BTC, indicating that as a consequence of the precipitation of calcite there is a transition from Fickian to non-Fickian or anomalous transport behavior. This can be explained by the development of zones with varying hydraulic conductivities induced by the growth of the calcite mineral, as depicted in Figure 5c. These zones are characterized by areas of low permeability, represented by elongated carbonate structures, and areas of high permeability, which serve as preferential flow channels. The earlier arrival of the tracer after the MDP phase results from the acceleration of flow within preferential channels, where the local velocity increases as the effective flow area decreases, together with flow through unaltered (non-precipitated) regions. The reduction of concentrations in the first arrival, the presence of a second peak, and the extended tailing of the BTC are due to accumulation of the tracer in areas where calcite precipitated (elongated carbonate structures), which act as zones of low permeability with reduced velocities, which in general have the potential to store the solute for longer periods of time. The solute that during early stages diffused into the low permeability zones slowly diffuses back into the main flow channel at late times.

 doi:10.20944/preprints202601.2390.v1

This release mechanism causes the concentration to decline slowly, explaining the long tail in the breakthrough curve. These results suggest that the breakthrough curve obtained after the MDP phase reflects a self-organized heterogeneous porous medium (development of heterogeneity that arises from internal feedbacks between flow, solute transport, and calcite precipitation, rather than from externally imposed parameter variations) characterized by highly anisotropic, spatially correlated variations in local hydraulic conductivity, oriented along the mean flow velocity, which leads to a more heterogeneous water velocity field. The latter may be characterized by a higher dispersion coefficient giving a higher precipitation rate as illustrated by equation (3). However, this would still result in BTCs of Fickian behavior. That is, a model, that increases the dispersion coefficient according to precipitated calcite, will not reproduce the two peaks of the observed BTC. More promising are models that use MRMT (Multi Rate Mass Transfer), a method for reproducing non-Fickian behavior. For instance, Wang et al. [62] have successfully applied MRMT to biofilm growth in porous media and its effect on transport properties.

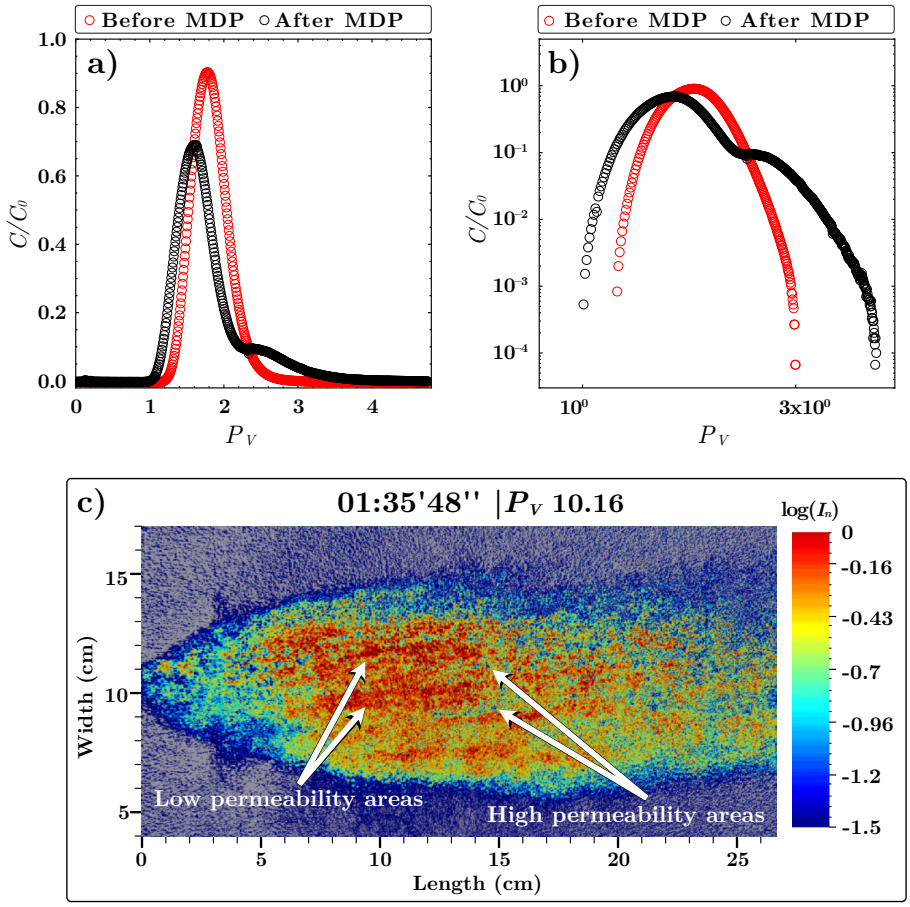

Figure 5. a) Breakthrough curves obtained before and after MDP experiment. Concentration values are normalized in terms of $\frac{C}{C_0}$, and time is expressed in pore volume P_v. The red and black curve represents solute transport before (T_1) and after (T_2) Mixing-Driven Precipitation (MDP) experiment. b) Experimental breakthrough curves expressed on a logarithmic scale. c) Map of calcite precipitation expressed semi-quantitatively in $\log(I_n)$ showing elongated carbonate structures patterns and preferential flow paths.

4. Conclusions

Mineral precipitation driven by mixing modifies the properties of porous media influencing flow and transport processes. Understanding how precipitation structures form and impact solute behavior is crucial for environmental and groundwater engineering applications such as pollutant remediation and carbon sequestration. In this regard, breakthrough curves (BTCs) are essential tools for analyzing changes in transport behavior. Optimal conditions for promoting precipitation structures have been

 doi:10.20944/preprints202601.2390.v1

historically studied in carbonate systems. However, the mechanisms underlying the spatiotemporal evolution of carbonate structure patterns and their influence on solute transport remains largely unknown. In this context, we presented a precipitation experiment conducted in a two-dimensional, intermediate-scale synthetic aquifer designed to resemble a coarse sand aquifer system. In this study, we investigated the Mixing-Driven Precipitation (MDP) of calcite and evaluated its impact on solute transport through breakthrough curves. Finally, we conclude that:

1. After conducting the MDP experiment, a self-organized heterogeneous precipitation pattern emerges, characterized by elongated carbonate structures that created markedly preferential flow paths, aligned with the main flow direction. The precipitation front formed a symmetrical bell-shaped curve located at the middle of the tank, a pattern distinctly different from the asymmetrical shape predicted by a homogeneous well-mixed equilibrium model with constant transport and hydraulic properties. Initial homogeneity assumed by many theoretical models overly simplifies reality and thus affect the predicted distribution of precipitation, as demonstrated by the comparison of experimental results with the semi-analytical model.
2. The highest rate of calcite precipitation occurred within a short period of time at the beginning of the MDP experiment, suggesting that the system is highly sensitive to initial perturbations. Fluctuations in the measured outlet pH values suggest changes in the local flow direction, associated to the precipitation of calcite. Interestingly, a significant effect on permeability and transport was achieved with a relatively small amount of precipitated calcite (less than 0.1% of the total tank volume).
3. MDP shifted the solute transport behavior of the system from a classical Fickian homogeneous to a non-Fickian anomalous pattern. This was evidenced by a conservative breakthrough curve with a double-peak and pronounced tailing, indicative of channeling and back-diffusion processes from low permeability zones.

Our results underscore the importance of understanding the mechanisms behind the formation of local pore-scale heterogeneities due to precipitation, as well as the resulting macroscopic precipitation structure, in order to accurately analyze the behavior of coarse granular aquifers following mineral precipitation processes. This finding highlights the need for models that capture the spatial heterogeneity of precipitation for an accurate interpretation of tracer tests. Future research aimed at improving the understanding of breakthrough curves must focus on accurately characterizing the heterogeneous nature of mineral precipitation patterns.

Author Contributions: G.G.-S.: conceptualization, formal analysis, investigation, methodology, software, validation, visualization, and writing—original draft preparation; R.P.-I.: conceptualization, formal analysis, methodology, software, supervision, visualization, and writing—review & editing; M.W.S.: conceptualization, formal analysis, methodology, software, and writing—review & editing; D.R.-N.: conceptualization, investigation, methodology, and visualization; M.T.: conceptualization, methodology, and writing—review & editing; D.F.-G.: conceptualization, formal analysis, methodology, resources, supervision, and writing—review & editing. All authors have read and agreed to the published version of the manuscript.

Funding: This research was funded by the Ministry of Economic Affairs and Digital Transformation of the Government of Spain (GRADIENT, PID2021-127911OB-I00), the State Agency for Research (AGAUR-SGR-609) of the Generalitat de Catalunya, and the International Doctoral Scholarship Program of Chile, managed by ANID (National Research and Development Agency).

Data Availability Statement: Data will be made available on request.

Acknowledgments: The authors thank Maria Llinàs Griful of the Universitat Politècnica de Catalunya for her invaluable support during the laboratory work.

Conflicts of Interest: The authors declare no conflicts of interest.

 doi:10.20944/preprints202601.2390.v1

References

1. Rodríguez-Escales, P.; Fernàndez-Garcia, D.; Drechsel, J.; Folch, A.; Sanchez-Vila, X. Improving degradation of emerging organic compounds by applying chaotic advection in m anaged a quifer r echarge in randomly heterogeneous porous media. *Water Resources Research* **2017**, *53*, 4376–4392.
2. Wang, Y.; Fernàndez-Garcia, D.; Sole-Mari, G.; Rodríguez-Escales, P. Enhanced NAPL removal and mixing with engineered injection and extraction. *Water Resources Research* **2022**, *58*, e2021WR031114.
3. Bertran, O.; Fernàndez-Garcia, D.; Sole-Mari, G.; Rodríguez-Escales, P. Enhancing Mixing During Groundwater Remediation via Engineered Injection-Extraction: The Issue of Connectivity. *Water Resources Research* **2023**, *59*, e2023WR034934.
4. Yuan, L.; Wang, K.; Zhao, Q.; Yang, L.; Wang, G.; Jiang, M.; Li, L. An overview of in situ remediation for groundwater co-contaminated with heavy metals and petroleum hydrocarbons. *Journal of Environmental Management* **2024**, *349*, 119342.
5. Sanford, W.E.; Konikow, L.F. Porosity development in coastal carbonate aquifers. *Geology* **1989**, *17*, 249–252.
6. Yabusaki, S.; Cantrell, K.; Sass, B.; Steefel, C. Multicomponent reactive transport in an in situ zero-valent iron cell. *Environmental Science & Technology* **2001**, *35*, 1493–1503.
7. Johnson, J.W.; Nitao, J.J.; Knauss, K.G. Reactive transport modelling of CO2 storage in saline aquifers to elucidate fundamental processes, trapping mechanisms and sequestration partitioning. *Geological Society, London, Special Publications* **2004**, *233*, 107–128.
8. Werth, C.J.; Cirpka, O.A.; Grathwohl, P. Enhanced mixing and reaction through flow focusing in heterogeneous porous media. *Water Resources Research* **2006**, *42*.
9. Dentz, M.; Le Borgne, T.; Englert, A.; Bijeljic, B. Mixing, spreading and reaction in heterogeneous media: A brief review. *Journal of contaminant hydrology* **2011**, *120*, 1–17.
10. de Dreuzy, J.R.; Carrera, J.; Dentz, M.; Le Borgne, T. Time evolution of mixing in heterogeneous porous media. *Water resources research* **2012**, *48*.
11. Dentz, M.; Hidalgo, J.J.; Lester, D. Mixing in porous media: concepts and approaches across scales. *Transport in Porous Media* **2023**, *146*, 5–53.
12. Anna, P.d.; Jimenez-Martinez, J.; Tabuteau, H.; Turuban, R.; Le Borgne, T.; Derrien, M.; Méheust, Y. Mixing and reaction kinetics in porous media: An experimental pore scale quantification. *Environmental science & technology* **2014**, *48*, 508–516.
13. Valocchi, A.J.; Bolster, D.; Werth, C.J. Mixing-limited reactions in porous media. *Transport in Porous Media* **2019**, *130*, 157–182.
14. Rolle, M.; Le Borgne, T. Mixing and reactive fronts in the subsurface. *Reviews in Mineralogy and Geochemistry* **2019**, *85*, 111–142.
15. Tartakovsky, A.M.; Tartakovsky, G.D.; Scheibe, T.D. Effects of incomplete mixing on multicomponent reactive transport. *Advances in Water Resources* **2009**, *32*, 1674–1679.
16. Wright, E.E.; Richter, D.H.; Bolster, D. Effects of incomplete mixing on reactive transport in flows through heterogeneous porous media. *Physical Review Fluids* **2017**, *2*, 114501.
17. Battiato, I.; Tartakovsky, D.M.; Tartakovsky, A.M.; Scheibe, T. On breakdown of macroscopic models of mixing-controlled heterogeneous reactions in porous media. *Advances in water resources* **2009**, *32*, 1664–1673.
18. Lee, M.; Paik, I.S.; Kim, I.; Kang, H.; Lee, S. Remediation of heavy metal contaminated groundwater originated from abandoned mine using lime and calcium carbonate. *Journal of hazardous materials* **2007**, *144*, 208–214.
19. Laumann, S.; Micić, V.; Lowry, G.V.; Hofmann, T. Carbonate minerals in porous media decrease mobility of polyacrylic acid modified zero-valent iron nanoparticles used for groundwater remediation. *Environmental Pollution* **2013**, *179*, 53–60.
20. Wang, Y.; Pleasant, S.; Jain, P.; Powell, J.; Townsend, T. Calcium carbonate-based permeable reactive barriers for iron and manganese groundwater remediation at landfills. *Waste management* **2016**, *53*, 128–135.
21. Mohapatra, A.K.; Sujathan, S.; Ekamparam, A.S.; Singh, A. The role of manganese carbonate precipitation in controlling fluoride and uranium mobilization in groundwater. *ACS Earth and Space Chemistry* **2021**, *5*, 2700–2714.
22. Rosenbauer, R.J.; Koksalan, T.; Palandri, J.L. Experimental investigation of CO2–brine–rock interactions at elevated temperature and pressure: Implications for CO2 sequestration in deep-saline aquifers. *Fuel processing technology* **2005**, *86*, 1581–1597.

 doi:10.20944/preprints202601.2390.v1

23. Kharaka, Y.K.; Thordsen, J.J.; Hovorka, S.D.; Nance, H.S.; Cole, D.R.; Phelps, T.J.; Knauss, K.G. Potential environmental issues of CO2 storage in deep saline aquifers: Geochemical results from the Frio-I Brine Pilot test, Texas, USA. *Applied Geochemistry* **2009**, *24*, 1106–1112.
24. Altman, S.J.; Aminzadeh, B.; Balhoff, M.T.; Bennett, P.C.; Bryant, S.L.; Cardenas, M.B.; Chaudhary, K.; Cygan, R.T.; Deng, W.; Dewers, T.; et al. Chemical and hydrodynamic mechanisms for long-term geological carbon storage. *The Journal of Physical Chemistry C* **2014**, *118*, 15103–15113.
25. Keith, D.C.; Harrison, W.J.; Wendlandt, R.F.; Daniels, E.J. Mineralogical responses of siliciclastic carbonate-cemented reservoirs to steamflood enhanced oil recovery. *Applied geochemistry* **1998**, *13*, 491–507.
26. Cuthbert, M.O.; McMillan, L.A.; Handley-Sidhu, S.; Riley, M.S.; Tobler, D.J.; Phoenix, V.R. A field and modeling study of fractured rock permeability reduction using microbially induced calcite precipitation. *Environmental science & technology* **2013**, *47*, 13637–13643.
27. Wu, J.; Wang, X.B.; Wang, H.F.; Zeng, R.J. Microbially induced calcium carbonate precipitation driven by ureolysis to enhance oil recovery. *RSC advances* **2017**, *7*, 37382–37391.
28. Alarifi, S.A.; Mustafa, A.; Omarov, K.; Baig, A.R.; Tariq, Z.; Mahmoud, M. A review of enzyme-induced calcium carbonate precipitation applicability in the oil and gas industry. *Frontiers in Bioengineering and Biotechnology* **2022**, *10*, 900881.
29. Mitchell, A.C.; Ferris, F.G. The coprecipitation of Sr into calcite precipitates induced by bacterial ureolysis in artificial groundwater: temperature and kinetic dependence. *Geochimica et Cosmochimica Acta* **2005**, *69*, 4199–4210.
30. Singh, R.; Yoon, H.; Sanford, R.A.; Katz, L.; Fouke, B.W.; Werth, C.J. Metabolism-induced CaCO3 biomineralization during reactive transport in a micromodel: Implications for porosity alteration. *Environmental science & technology* **2015**, *49*, 12094–12104.
31. Singurindy, O.; Berkowitz, B.; Lowell, R.P. Carbonate dissolution and precipitation in coastal environments: Laboratory analysis and theoretical consideration. *Water Resources Research* **2004**, *40*.
32. Fujita, Y.; Taylor, J.L.; Gresham, T.L.; Delwiche, M.E.; Colwell, F.S.; McLing, T.L.; Petzke, L.M.; Smith, R.W. Stimulation of microbial urea hydrolysis in groundwater to enhance calcite precipitation. *Environmental science & technology* **2008**, *42*, 3025–3032.
33. Lauchnor, E.G.; Schultz, L.N.; Bugni, S.; Mitchell, A.C.; Cunningham, A.B.; Gerlach, R. Bacterially induced calcium carbonate precipitation and strontium coprecipitation in a porous media flow system. *Environmental science & technology* **2013**, *47*, 1557–1564.
34. Tartakovsky, A.M.; Redden, G.; Lichtner, P.C.; Scheibe, T.D.; Meakin, P. Mixing-induced precipitation: Experimental study and multiscale numerical analysis. *Water Resources Research* **2008**, *44*.
35. Zhang, C.; Dehoff, K.; Hess, N.; Oostrom, M.; Wietsma, T.W.; Valocchi, A.J.; Fouke, B.W.; Werth, C.J. Pore-scale study of transverse mixing induced CaCO3 precipitation and permeability reduction in a model subsurface sedimentary system. *Environmental science & technology* **2010**, *44*, 7833–7838.
36. Katz, G.E.; Berkowitz, B.; Guadagnini, A.; Saaltink, M.W. Experimental and modeling investigation of multicomponent reactive transport in porous media. *Journal of contaminant hydrology* **2011**, *120*, 27–44.
37. Yoon, H.; Valocchi, A.J.; Werth, C.J.; Dewers, T. Pore-scale simulation of mixing-induced calcium carbonate precipitation and dissolution in a microfluidic pore network. *Water Resources Research* **2012**, *48*.
38. Bray, J.M.; Lauchnor, E.G.; Redden, G.D.; Gerlach, R.; Fujita, Y.; Codd, S.L.; Seymour, J.D. Impact of mineral precipitation on flow and mixing in porous media determined by microcomputed tomography and MRI. *Environmental Science & Technology* **2017**, *51*, 1562–1569.
39. Rolle, M.; Eberhardt, C.; Chiogna, G.; Cirpka, O.A.; Grathwohl, P. Enhancement of dilution and transverse reactive mixing in porous media: Experiments and model-based interpretation. *Journal of contaminant hydrology* **2009**, *110*, 130–142.
40. Li, X.; Yang, X. Effects of physicochemical properties and structural heterogeneity on mineral precipitation and dissolution in saturated porous media. *Applied Geochemistry* **2022**, *146*, 105474.
41. Cil, M.B.; Xie, M.; Packman, A.I.; Buscarnera, G. Solute mixing regulates heterogeneity of mineral precipitation in porous media. *Geophysical Research Letters* **2017**, *44*, 6658–6666.
42. Perkins, T.K.; Johnston, O. A review of diffusion and dispersion in porous media. *Society of Petroleum Engineers Journal* **1963**, *3*, 70–84.
43. Parkhurst, D.L.; Appelo, C. User's guide to PHREEQC (Version 2): A computer program for speciation, batch-reaction, one-dimensional transport, and inverse geochemical calculations. Technical report, US Geological Survey, 1999.

 doi:10.20944/preprints202601.2390.v1

44. Bradski, G.; Kaehler, A. *Learning OpenCV: Computer vision with the OpenCV library*; " O'Reilly Media, Inc.", 2008.
45. Howse, J. *OpenCV computer vision with python*; Vol. 27, Packt Publishing Birmingham, UK, 2013.
46. Schuszter, G.; Brau, F.; De Wit, A. Calcium carbonate mineralization in a confined geometry. *Environmental Science & Technology Letters* **2016**, *3*, 156–159.
47. Schuszter, G.; De Wit, A. Comparison of flow-controlled calcium and barium carbonate precipitation patterns. *The Journal of Chemical Physics* **2016**, *145*.
48. Schuszter, G.; Brau, F.; De Wit, A. Flow-driven control of calcium carbonate precipitation patterns in a confined geometry. *Physical Chemistry Chemical Physics* **2016**, *18*, 25592–25600.
49. De Simoni, M.; Sanchez-Vila, X.; Carrera, J.; Saaltink, M. A mixing ratios-based formulation for multicomponent reactive transport. *Water Resources Research* **2007**, *43*.
50. Wexler, E.J. *Analytical solutions for one-, two-, and three-dimensional solute transport in ground-water systems with uniform flow*; US Government Printing Office, 1992.
51. Parkhurst, D.L. *User's guide to PHREEQC: A computer program for speciation, reaction-path, advective-transport, and inverse geochemical calculations*; Number 95-4227, US Department of the Interior, US Geological Survey, 1995.
52. Parkhurst, D.L.; Appelo, C.; et al. Description of input and examples for PHREEQC version 3—a computer program for speciation, batch-reaction, one-dimensional transport, and inverse geochemical calculations. *US geological survey techniques and methods* **2013**, *6*, 497.
53. Noiriel, C.; Steefel, C.I.; Yang, L.; Bernard, D. Effects of pore-scale precipitation on permeability and flow. *Advances in water resources* **2016**, *95*, 125–137.
54. Leroy, P.; Li, S.; Jougnot, D.; Revil, A.; Wu, Y. Modelling the evolution of complex conductivity during calcite precipitation on glass beads. *Geophysical Journal International* **2017**, *209*, 123–140.
55. Nambi, I.M.; Werth, C.J.; Sanford, R.A.; Valocchi, A.J. Pore-scale analysis of anaerobic halorespiring bacterial growth along the transverse mixing zone of an etched silicon pore network. *Environmental science & technology* **2003**, *37*, 5617–5624.
56. Green, D.C.; Shida, Y.; Honma, N.; Holden, M.A.; Kim, Y.Y.; Kulak, A.N.; Ogasawara, W.; Meldrum, F.C. Skin-Deep Surface Patterning of Calcite. *Chemistry of Materials* **2019**, *31*, 8725–8733.
57. Izumoto, S.; Huisman, J.A.; Zimmermann, E.; Heyman, J.; Gomez, F.; Tabuteau, H.; Laniel, R.; Vereecken, H.; Méheust, Y.; Le Borgne, T. Pore-scale mechanisms for spectral induced polarization of calcite precipitation inferred from geo-electrical millifluidics. *Environmental Science & Technology* **2022**, *56*, 4998–5008.
58. Redden, G.; Fujita, Y.; Delwiche, M.; White, T.; Roney, T.; Versteeg, R.; Fox, D.; Palmer, C. Mixing solutions, precipitation and changing permeability in porous media. *Geochimica et Cosmochimica Acta Supplement* **2005**, *69*, A180.
59. Bray, J.M.; Lauchnor, E.G.; Redden, G.D.; Gerlach, R.; Fujita, Y.; Codd, S.L.; Seymour, J.D. Impact of Mineral Precipitation on Flow and Mixing in Porous Media Determined by Microcomputed Tomography and MRI. *Environmental Science & Technology* **2017**, *51*, 1562–1569. PMID: 28001377, https://doi.org/10.1021/acs.est.6b02999.
60. Gramling, C.M.; Harvey, C.F.; Meigs, L.C. Reactive transport in porous media: A comparison of model prediction with laboratory visualization. *Environmental science & technology* **2002**, *36*, 2508–2514.
61. Borgne, T.L.; Ginn, T.R.; Dentz, M. Impact of fluid deformation on mixing-induced chemical reactions in heterogeneous flows. *Geophysical Research Letters* **2014**, *41*, 7898–7906.
62. Wang, J.; Carrera, J.; Saaltink, M.W.; Petchamé-Guerrero, J.; Herrera, G.S.; Valhondo, C. Biofilm growth in porous media well approximated by fractal multirate mass transfer with advective-diffusive solute exchange. *Water Resources Research* **2024**, *60*, e2023WR036872.